Available online at www.sciencedirect.com
SCIENCE DIRECT
Polymer 46 (2005) 8266–8274
polymer
www.elsevier.com/locate/polymer

Nanoscale fibrillar crystals of PET from dilute quiescent solution

Y. Ma, U.S. Agarwal*, X.N. Yang, X. Zheng, J. Loos, M.M.R.M. Hendrix, O.L.J. van Asselen, P.J. Lemstra

Faculty of Chemical Engineering, Polymer Technology Group/Dutch Polymer institute, Eindhoven University of Technology, 5600 MB Eindhoven, The Netherlands

Received 24 February 2005; received in revised form 19 May 2005; accepted 10 June 2005
Available online 21 July 2005

Abstract

The crystallization behavior of poly(ethylene terephthalate) (PET, IV ~ 2 dL/g) from solution in biphenyl–diphenyl ether mixed solvent is examined. Reversible gelation of the polymer solution is observed during cooling of the solutions. Light scattering and DSC analysis are used to follow the heating and cooling processes, thus determining the crystallization temperature and the melting point, which are found to be nearly independent of the polymer concentration (0.25–5%). High degree of crystallization (>50%) is observed in the PET crystallized from the solution at 170 °C. Morphological characteristics of the crystals obtained after solvent removal are determined by WAXD, FTIR, SEM and TEM examination. The crystallization of PET into unique high aspect ratio fibrillar morphology during cooling of the solutions explains their gelation even at low PET concentration. Thin films made from the thus obtained PET could be drawn five times at 250 °C, resulting in only moderate values of modulus and strength.

Keywords: Poly(ethylene terephthalate); Nanofibrillar; Solvent induced crystallization

1. Introduction

Poly(ethylene terephthalate) (PET) is one of the commercially most important polymers, the major applications being textile fibers, soft drink bottles, injection molding, tire cord filaments and industrial fibers. While PET of IV ~ 0.6 dL/g obtained by melt polymerization is sufficient for textile fiber applications, the other applications demand solid state polymerization (SSP) to IV ~ 1.0 dL/g [1–6]. An even higher extent of post-polymerization to IV as high as 3 dL/g is desired for its solution spinning leading to potentially high modulus high strength fibers [7–9].

Crystallization of polymers from entangled melts and concentrated solutions leads to crystallites that are highly interconnected by tie molecules. However, when a dilute solution of a crystallizable polymer is cooled under controlled conditions, the polymer may crystallize as single crystals. Since the discovery of polyethylene crystallization from dilute solutions into lamellar crystals, crystallization of several other important polymers such as polyvinyl chloride, carrageenen, polyamides and syndiotactic polystyrene has been carried out in solution, and found to display special chain conformations leading to a variety of crystalline morphology [10]. While suspensions of lamellar crystals are often formed, crystallization from solutions under suitable conditions can result in thermoreversible gelation wherein small crystallites serve as entanglements points between flexible polymer molecules forming the network [11,12]. For example, cooling of polyethylene in xylene solution results in a suspension of crystals, and stirring of the solution at high concentration results in formation of transparent elastic gels with shish-kebab crystalline morphology. These gels enable processing into useful materials, such as ultra strong fibers [13]. Reversible gelation can also occur in absence of crystallization through other forms of interchain binding [14].

Several workers have examined solvent induced crystallization in PET [15–18]. In addition, crystallization of PET from solutions in oligomeric PEO has been studied in recent years, albeit only for concentrated (10–30%) solutions [19–21]. Oh et al. [22] studied the influence of PET concentration (5–50%) and molecular weight

* Corresponding author. Tel.: +31 40 247 3079.
E-mail address: u.s.agarwal@tue.nl (U.S. Agarwal).

0032-3861/$ - see front matter © 2005 Elsevier Ltd. All rights reserved.
doi:10.1016/j.polymer.2005.06.065

(IV = 0.6–2.13 dL/g) on the crystallization and melting transitions in nitrobenzene. Crystallization of PET on microscope grid during solvent evaporation from dilute solutions in benzyl alcohol at room temperature was reported to result in fibrillar growth, by laydown of molecules along the growing fibril [23]. Crystallization kinetics of PET from solutions *N*-methyl-2-pyrrolidinone at elevated temperatures was studied, but without reference to crystal morphology [24]. Sun et al. [25] examined the crystallization potential of PET extracted from suddenly quenched solution in phenol, and concluded that the higher crystallization potential of the freeze–dried PET as compared to solution cast PET is related to the reduced entanglements in the former. Considering the possible influence of such crystal morphology on polymer properties, we here examine crystallization behavior of PET from its solution in the thermic fluid: The mixed solvent of diphenyl ether and biphenyl.

2. Experimental

2.1. Materials

Cylindrical PET chips (diameter 1.1 mm, length 2.8 mm, IV ~ 2.1 dL/g) were obtained from Acordis Research (Arnhem, The Netherlands), and predried at 150 °C under vacuum for 4 h before use. Diphenyl ether (99%) and biphenyl (99%) from Merck were used as received, and mixed at 73.5:26.5 (w:w) ratio to make the mixed solvent (DPE–BP). The solvent mixture DPE–BP was dried over molecular sieves for at least 2 days.

2.2. Detection of phase transition by light scattering

Predried PET was dissolved at the desired concentration in the DPE–BP mixture by stirring under argon atmosphere in a 20 mL glass bottle, at 240 °C in a molten salt bath. A preheated (240 °C) glass capillary with rectangular cross section (Vitrotube 3520 made by VitroCom Inc., wall thickness 0.2 mm, inner size 0.2 mm, width 2.0 mm) was introduced with its open end downwards, so as to dip the open end into the solution. When part of the solution seeped into the glass capillary by capillary action, the capillary was withdrawn and sealed at the open ends. The capillary was mounted on a hot stage (Linkam THMS600/TMS93) and laser light (Melles Griot 05-LHR-991, 30 mW, 632 nm) was shined on it from a distance of 10 cm, while the scattering was measured with a silicon PIN type photodiode detector (Centrovision, Model BPW 34) placed at 10 cm from the sample and connected to an XY plotter (Kipp & Zonen, Model BD 40). The sample was subjected to the following program with the hot stage: Heating from 60 to 240 °C at 20 °C/min, isothermal for 5 min, cooling at 20 °C/min to 50 °C, isothermal for 5 min, and heating at 20 °C/min to 275 °C.

2.3. Isothermal crystallization from solution

PET was dissolved at the desired concentration in the DPE–BP by stirring in a test tube at 240 °C in a molten salt bath over 1 h. The test tube was transferred to a silicon oil bath maintained at 170 °C. With passage of time, the solution turned turbid and the test tube was withdrawn from the hot bath after 2 h when no further increase in turbidity could be observed.

2.4. Film formation and drawing from solution crystallized PET

PET (1.0 g) was dissolved in DPE–BP at the desired concentration (0.2 wt%) at 240 °C, crystallized isothermally at 170 °C, and filtered using Whattman 595 filter. Excess solvent was allowed to drain over 1 h. The loosely interconnected gel left on the filter paper was laid out in form of a 2 mm thick sheet on another filter paper supported on a metal wire mesh placed in a glass petri-dish. The sheet was covered with another filter paper and then with another wire mesh, to maintain the dimension of the sheet. Acetone is added to the petri-dish to allow extraction of the solvent DPE–BP overnight. After pouring out the solvents, the petri-dish was transferred to a vacuum oven, and maintained at 100 °C for 24 h. Dried film of thickness 0.15 mm was then easily separated form the filter papers and wire–mesh screens.

A small part of the film was subjected to IV measurement. Since the film was brittle, it was subjected to constrained annealing between stainless steel plates at 220 °C for 2 min. Sharp blade was used to cut out 1 mm wide strips. The ends of the strip were held between fingers, enabling us to apply tensile stress, and then bring the central parts of the strip to contact a hotbench (Kofler Heizbank, Model 7841) at 250 °C. Following the quick heating, the strip stretched to a draw ratio of about 5–6 in about 5 s. The drawn samples were weighed to determine their cross section, and tested for their tensile properties using Zwick Z010 with 20 N load cell, sample span of 1 cm and extension rate of 0.5 cm/min.

2.5. DSC

The melting and crystallization characteristics of the samples were examined using Perkin–Elmer differential scanning calorimetry system DSC-7. The heat of melting and heat of crystallization were determined from the corresponding peak area during heating and cooling scans at 20 °C/min.

2.6. WAXD

The crystallized PET samples were dried by evaporation under vacuum at room temperature. The WAXD measurements were carried out with a Rigaku D/Max-B

diffractometer, using Cu K_α radiation at 40 kV and 30 mA. The samples were measured with a step size of 0.02 ($^\circ 2\theta$) and a dwell time of 2 (s).

2.7. Intrinsic viscosity determination

The relative viscosity (η_{rel}) of solution of PET in phenol–TCE mixture (1:1, by weight) at concentration ($c = 0.5$ g/dL) was determined using ubbelohde viscometer at 30 °C. IV was estimated from this single point measurement of η_{rel} and using the following approximation for linear flexible chains [26]:

$$\mathrm{IV} = \frac{1}{c}[2(\eta_{rel} - 1) - 2\ln(\eta_{rel})]^{1/2}$$

2.8. Scanning electron microscopy

Following the isothermal crystallization from solution (Section 2.3), a sample of the turbid suspension was withdrawn with a spatula, mounted on a freshly cleaved mica sheet, and dried by evaporation at 70 °C in a vacuum oven. The SEM was carried out on a Philips filed-emission environmental scanning electron microscope XL30 ESEM–FEG equipped with a field emission electron source. The acceleration voltage used for image acquisition was 2 kV.

2.9. Transmission electron microscopy

Following the isothermal crystallization from solution (Section 2.3), a droplet of the turbid suspension was cast onto a copper TEM grid coated with a thin layer of amorphous carbon, dried by evaporation at 70 °C in a vacuum oven overnight. Bright-field (BF) TEM morphology observations and acquisition of selected-area electron diffraction (SAED) patterns were conducted on a JEOL JEM-2000FX transmission electron microscope operated at 80 kV. Traditional negative plates were used to record all the images. The negatives were digitized using a high-resolution scanner (Agfa DUO scanner), working in gray mode with 8 bits/channel of gray scale.

2.10. Preparation of solid state crystallized PET

Highly crystalline PET chips were prepared from PET chips (IV ~ 0.6 dL/g) by pressing at 150 °C into 180 μm films, and then precrystallization at 165 °C for 6 h followed by solid state polymerization at 250 °C for 4 h to IV = 2.2 dL/g [6].

2.11. Fiber formation from concentrated PET solution

Concentrated solution (30 wt%) of PET (IV = 1.8 dL/g) in DPE–BP at 250 °C was obtained by solution polymerization as described in our earlier work [27]. Filaments (diameter ~200 μm) were drawn out while quickly withdrawing a metal wire tip dipped in this solution. These filaments were dried overnight at 150 °C under vacuum, and then drawn at 240 °C using the hotbench (Kofler Heizbank, Model 7841) to a draw ratio of 7. The drawn samples were weighed to determine their cross section, and tested for their tensile properties using Zwick Z010 with 20 N load cell, sample span of 1 cm and extension rate of 0.5 cm/min.

3. Results and discussion

The most common thermoreversible gelation in polymer solutions is due to crystallization occurring due to under cooling. The onset of crystallization (T_c) may depend on many factors such as cooling rate and polymer concentration, besides the polymer-solvent characteristics. The melting temperature (T_m) of these crystals may depend on T_c, and is greater than T_c. Presence of solvent can decrease T_m. Another phenomena that can lead to gelation is the liquid–liquid phase separation, which can precede crystallization of the concentrated phase [28]. We are interested in examining the gelation taking place during cooling of dilute PET solutions.

3.1. Detection of phase transition

When a polymer crystallizes from a dilute solution, the solid crystallites thus formed may remain suspended in the solvent, giving a turbid appearance. Formation of such crystallites, or a liquid–liquid phase separation can both be detected by examining the scattering behavior of polymer solutions. Fig. 1 shows the scattering response to an incident laser beam on the PET solutions of various concentrations during a cooling and a heating cycle. During the cooling cycle, the onset of scattering is seen at ~165 °C, possibly indicating the crystallization of PET at this T_c. During the subsequent heating cycle, the scattering intensity decreases at T_m ~ 204 °C, indicating the possible melting of PET

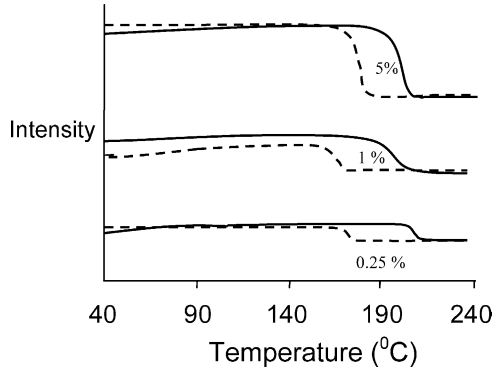

Fig. 1. Scattering during heating and cooling of PET solution of shown concentrations, in response to incident laser beam. Temperature profile: Heating from 40 to 240 °C at 20 °C/min (solid lines), isothermal for 2 min, cooling at 20 °C/min to 40 °C (dashed lines).

crystals. The same transitions could be observed repeatedly during additional cooling and heating cycles, indicating thermoreversible nature of the involved processes. The T_m and T_c at the employed scanning rate (20 °C/min) are nearly independent of the polymer concentration.

Gelation characteristics of dilute PET solutions during cooling is also determined visually. PET solutions in DPE–BP at 240 °C at three different concentrations, 0.25, 1 and 5%, were step cooled from 240 °C by transferring to constant temperature bath maintained at 170 °C. Fig. 2 shows the appearance of these solutions after 1 h at 170 °C. While a settling suspension of a loosely interconnected swollen gel is seen in the 0.25% case, gelation is seen in the 1 and 5% solutions throughout the system. When the 0.25% solution–suspension was poured out from the test tubes into a petri-dish, we detected ~0.2 cm size translucent gel lumps suspended in the solvent. This gel was very soft as it could be easily deformed with a spatula, possibly indicating a low degree of entanglement between the crystallites. However, the 1% gel could support its own weight for 10 min at room temperature, as found by inverting the test tube.

3.2. Crystallization characteristics of PET from solution in DPE–BP

Fig. 3 shows the DSC scans of a gel obtained by natural cooling of a 10% PET solution in DPE–BP. Following the first heating to 275 °C, the subsequent cooling scan shows an exotherm with peak at 159.6 °C (T_c, $\Delta H_m = 5.55$ J/g), corresponding to the crystallization of PET. The low value of this T_c as compared to $T_c \sim 190$ °C of bulk PET (Fig. 4) can be attributed to higher degree of supercooling required to crystallize in presence of solvent. The subsequent heating scan shows an endotherm at 204.6 °C (T_m), corresponding to melting these PET crystals. The low value of the T_m as compared to bulk PET ($T_m \sim 250$ °C, Fig. 4) can be attributed to the presence of solvent during the DSC scan. The peaks at T_c and T_m are integrated to determine the heat of crystallization and heat of melting as 5.55 and 5.21 J/g, thus corresponding with the expected value for a sample

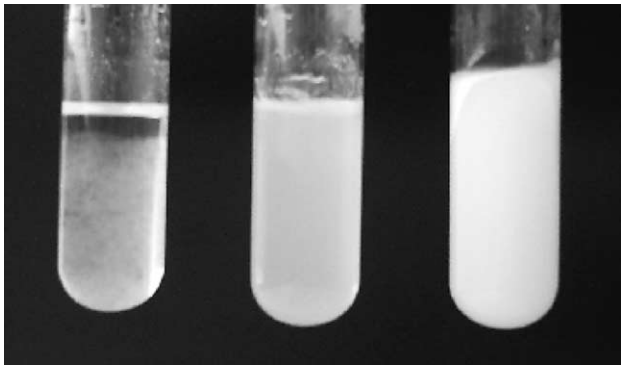

Fig. 2. Appearance of PET gels obtained by cooling PET solution of concentrations (0.25, 1.0 and 5%, from left to right) to 170 °C.

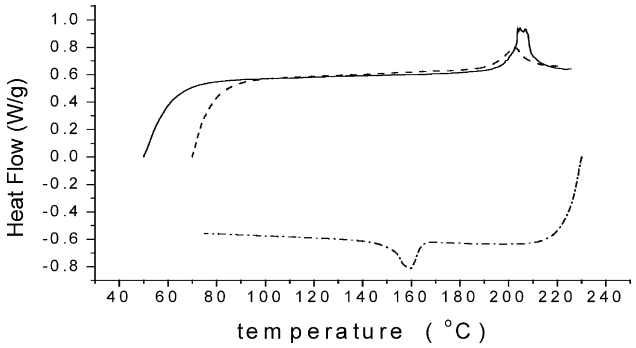

Fig. 3. DSC scans of a 10% PET gel in DPE–BP. First heating (50–230 °C, solid line), cooling (230–70 °C, lower dashed line) and second heating (70–2 °C, upper dotted line) scans are shown.

containing 10% PET with degree of crystallization x_c of about 50%, since the crystalline heat of melting of PET is 125.6 J/g [29]. The T_c and T_m values correspond very well with the scattering transitions (Fig. 1), indicating that the scattering is most likely resulting from crystallization.

It is interesting to determine if the crystallization precedes phase separation, or the crystallization occurs in the more concentrated phase following phase separation.

If a liquid–liquid phase separation precedes crystallization, then one would expect the phase separation temperature to depend on the polymer concentration [11]. However, onset of scattering (Fig. 1) and crystallization (Fig. 3) at 160–165 °C during the cooling, irrespective of the polymer concentration in the range 0.25–10%, indicates lack of such dependence at these concentrations. In addition, if a liquid–liquid phase separation precedes crystallization, then crystal size is expected to be limited to dimension of the concentrated phase. As we will see from microscopic examination, the crystals grown in dilute solutions (0.25%) display fibrillar morphology of very high aspect ratio, which

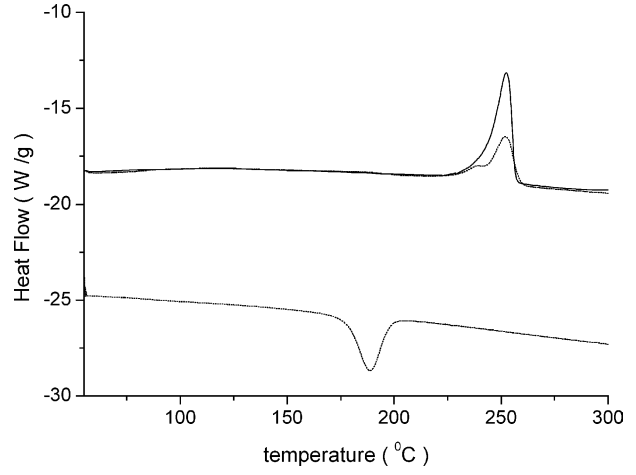

Fig. 4. DSC scans of an isothermally (170 °C) crystallized 0.25% PET gel in DPE–BP, after drying at room temperature under vacuum. First heating (50–300 °C, solid line), cooling (300–50 °C, lower dotted line) and second heating (50–300 °C, upper dotted line) scans are shown.

is unlikely to have resulted from a possible liquid–liquid phase separation.

The PET gel samples obtained by isothermal crystallization (170 °C) from solutions of three different concentrations (0.25, 1, and 5%) were dried by evaporation at room temperature under vacuum and subjected to DSC analysis. These three samples showed melting endotherms with peaks at 252.4, 252.7 and 251.6 °C, and with ΔH_m as 63.7, 64.4 and 64.1 J/g, respectively (Fig. 4). During subsequent cooling and heating of the 0.25% sample, we observe $T_c \sim 189$ °C and $T_m \sim 252$ °C with ΔH_c and ΔH_m each of 38 J/g (Fig. 4). These values are similar to the values for bulk crystallized PET, indicating that the structure formed during solution crystallization is lost during melting, as expected. In comparison, the ΔH_m of the dried gel samples during first heating was much higher (~ 64 J/g) and corresponds to $x_c \sim 51\%$. Such high degree of crystallization can be obtained in bulk PET samples also by annealing at $T \sim T_m$ for several hours [30], during gelation from concentrated solutions (10–30%) in oligomeric PEO [19–21], and during crystallization under high pressure [31,32].

3.3. Morphology of PET crystallized from solution in DPE–BP

Molecular packing of molecules in crystals is best determined by WAXD and electron diffraction. The following triclinic unit cell dimensions for PET have been reported [33–36]: $a = 0.448$ nm, $b = 0.585$ nm, $c = 1.075$ nm, $\alpha = 99.5°$, $\beta = 118.4°$, $\gamma = 111.2°$. For the $0\underline{1}1$, 010, $1\underline{1}1$, $1\underline{1}0$, 011, 100, $1\underline{1}1$ and 101 planes, the d-values are 0.537, 0.497, 0.4085, 0.386, 0.370, 0.340, 0.314, and 0.267, respectively. The chain alignment is along c-axis, along which the chain is nearly fully extended in a nearly planar conformation in the bc-plane. The $0\underline{1}1$ plane reflection is often used to roughly estimate the c-axis characteristics because of its only a small inclination with the c-axis [19,37].

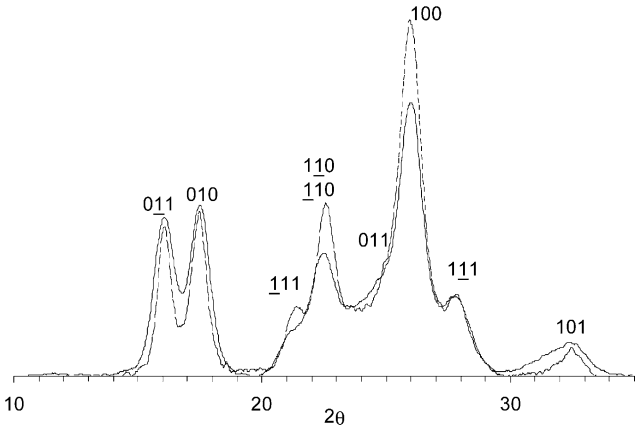

Fig. 5. Crystalline component of WAXD scans. Solid line: An isothermally (170 °C) crystallized 0.25% PET gel in DPE–BP, after drying at room temperature under vacuum. Dashed line: Solid state crystallized PET.

Fig. 5 shows a comparison of the WAXD patterns of the sample crystallized from 0.25% solution with the solid state polymerized sample (Section 2.10). The spectra have been corrected for Cu $K_{\alpha 2}$ and background scattering, and the amorphous spectrum has been subtracted while fitting the peaks by a Pearson-VII profile. The peaks are indexed according to the above known assignments. The solid state polymerized sample was chosen as the reference due to its comparable IV, and the desired high degree/order of crystallinity in the reference. The similar peak positions of the solid-state and solution crystallized samples indicates that the crystalline forms are identical. The X-ray determined degree of crystallization in the two samples is high: 60% for solution crystallized sample and 51% for SSP sample. This is in qualitative agreement with the DSC analysis which also showed higher crystallinity for the solution crystallized samples ($x_c = 0.5$), than for the solid state crystallized sample ($x_c = 0.38$). Higher crystallinity for PET crystallized from oligomeric PEO was also observed by Xue et al. [21] and Wang et al. [19]. An important difference between the two samples is the broadening of the $0\underline{1}1$ and 010 peaks for the solution crystallized sample as compared to the SSP sample, indicating smaller crystal size in the dilute solution crystallized PET as compared to the SSP PET. Calculation of the crystallite size $\bar{D}$ can be achieved by means of the Scherrer equation:

$$\bar{D} = \frac{0.9\lambda}{B \cos\theta}$$

where B is the full width at half maximum (FWHM) of the reflection peak determined after subtraction of the instrument broadening, the latter being determined independently with a standard reference material. The average crystallite size is determined by using a least squares fit to the FWHMs of the most distinct peaks: The ($0\underline{1}1$), (010), ($1\underline{1}0$), (100), ($1\underline{1}1$) and (101). The crystallite dimensions are thus calculated as 7.9 nm for the solution crystallized sample and 10.3 nm for the solid state crystallized sample. The smaller crystallite size of the solution crystallized sample is in agreement with its lower $T_m \sim 252$ °C as compared to $T_m \sim 260$ °C for the solid state crystallized sample. This is related to the annealing temperature that was very high (250 °C) for the solid state crystallized sample (Section 2.11). Smaller crystallite sizes for PET crystallized from oligomeric PEO, as compared to melt crystallized PET, was also observed by Wang et al. [19]. When the solution crystallized sample was annealed at 150 °C for several hours and then at 250 °C for 10 min, the corresponding crystallite dimension increased to 9.7 nm. The limitations on the crystallite dimension growth from annealing could also come from the fibril diameter, as we shall see from electron microscopy. In addition, we find that the fractional contribution of the area under the $0\underline{1}1$, 010 and 100 peaks to the total area under the crystalline curve are 0.15, 0.14 and 0.28 for the solution crystallized sample, as compared to 0.09, 0.11 and 0.34 for the solid state crystallized sample

(Fig. 5). Origin of this difference could lie in orientation of the WAXD samples. However, 2D pictures of the analyzed samples showed no orientation as inferred from the uniform intensity along the ring pattern.

Fig. 6(a) shows the scanning electron micrograph of the PET crystals obtained by isothermal crystallization (170 °C) of PET from a 0.25% solution in DPE–BP, followed by solvent evaporation on a mica sheet. Entire polymer appears to be present as fibrillar structures extending to lengths of several microns and width ~50–100 nm. While the fibrillar structure is formed in the bulk solution, their aggregation could be a result of the solvent evaporation process during the SEM sample preparation. The high aspect ratio (>100) of the crystals can explain the gelation of the solution by network formation at such a low concentration, as was also proposed for i-PS in decalin [38]. Formation of high aspect ratio fibrils can be explained by preferentially rapid growth of crystals along a certain lattice direction. The fibril ends in Fig. 6 appear blunt, rather than tapered as observed by Veld et al. [23] for crystallization on substrate while evaporating solvent. The blunt ends indicate that the crystal growth had occurred by laydown of molecules across the growing end. For the case of high PET concentration (5%), the SEM image (Fig. 6(b)) displays a continuous porous network of PET lamellar crystals, perhaps resulting from evaporation of the solvent distributed in a co-continuous manner.

It is known that lamellar crystals of nylon-66 can be grown from dilute solutions in lathlike shapes of thickness

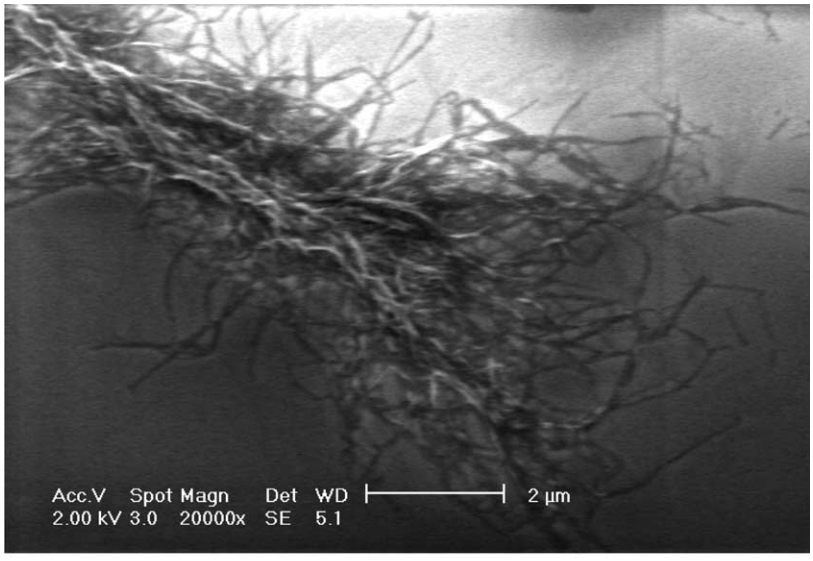

(a)

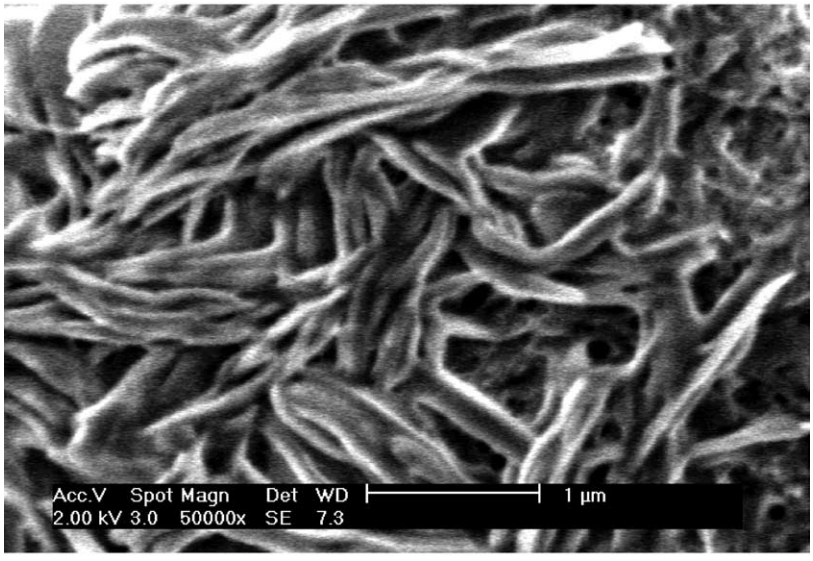

(b)

Fig. 6. SEM images of isothermally (170 °C) crystallized (a) 0.25% and (b) 5% PET solutions in DPE–BP, after drying at room temperature under vacuum.

5–6 nm [10,39] and nylon 10,10 was found to crystallize into lathlike, spindle like and planar sheet shapes [40]. Yang et al. [41] reported formation of micro fibrillar crystals (diameter 5–8 nm, length 50–300 nm) of nylon 10,10 also by atomizing its very dilute solution (0.0025–0.01%) and then crystallizing on amorphous carbon. While a fibrillar structure of polymer crystals exists extensively in natural and synthetic polymers crystallized in bulk [42], nanoscale separated fibrillar crystals have also been observed, e.g. through self assembly of peptides [43,44] templating in porous matrices [45], electrospinning [46], and dense grafting on linear backbones [47,48]. When induced by externally induced flow, crystallization from dilute solutions into fibrillar morphology is observed for several homopolymers, e.g. polyethylene [49,50], polyvinyl alcohol [51], polyethylene oxide [52], *cis*-1,4-polybutadiene [53], amylose [54] and Bombyx mori L. silk fibroin [55]. Alternatively, precipitation–crystallization of rigid highly aromatic polymers is known to result in fibrillar morphology with the chains alignment along the long axis of the fibrils [56,57]. In contrast, the PET microfibrils are obtained here by crystallization within dilute quiescent solution, and thus not on substrates during solvent evaporation.

The PET crystals grown from dilute solution (0.25%) were deposited on a carbon coated Cu-grid, and examined by TEM, when the fibrillar morphology (length several microns and width ~20 nm) of the solution grown crystals was observed again in the bright field (BF) TEM image (Fig. 7). The electron diffraction pattern of a selected area marked in Fig. 7 is shown as an inset in the same figure. There are at least three diffraction rings, corresponding to the *d*-spacings of 0.51, 0.43 and 0.35 nm (inner to outer ring). The innermost and the outermost rings are easily assigned as reflections from the 010 and 100 planes of known PET crystal structure [33]. However, we are unable to assign the intermediate ring to a specific plane, as it could belong to $1\underline{1}1$ or $1\underline{1}0$ reflections expected at 0.4085 and 0.386 nm, respectively. The position of the 010 arcs perpendicular to the fibrillar axis suggests that the crystalline *b*-axis is normal to the fibrillar axis. The position of the somewhat diffused 100 arcs on the outermost ring along the fibrillar axis suggests that the growth direction of the crystals is along the *a*-axis. This is consistent with the relatively blunt ends of the fibrils observed in the SEM (Fig. 6(a)) and the BF TEM images (Fig. 7), as the crystal growth occurred by laying down of the chain across the growing end, i.e. by adding chains by folding successively in the *a*-plane (or the *b*–*c* plane) [58]. The absence of the $01\underline{1}$ reflection may suggest *c*-axis alignment perpendicular to the supporting substrate. However, such a preferential alignment of *c*-axis is difficult to explain as the crystallization and fibril formation took place in bulk, thus in the absence of a surface influence. A larger fibril dimension along *b*-axis (as compared to along *c*-axis) could in principle result in the possible flat strips settling on their wider sides during solvent evaporation. However, imperfections during their settling would result in fibril width projection's variation over its length, which is seen for some fibrils in the SEM (Fig. 6(a)) and BF-TEM (Fig. 7) images. The then expected $01\underline{1}$ reflections in the electron diffraction could be either very weak or overlapping with the neighboring 010 reflection.

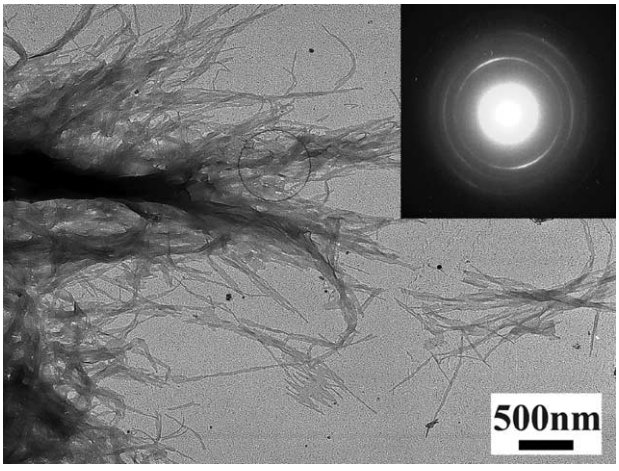

Fig. 7. Bright field TEM image of an isothermally (170 °C) crystallized 0.25% solution DPE–BP after drying at room temperature under vacuum. Inset: Electron diffraction pattern of the selected area marked as circle.

3.4. Mechanical properties of PET crystallized from dilute solution

The PET crystals grown from dilute solution (0.2%) were filtered and then dried at 100 °C to a film of thickness 0.15 mm (Section 2.4). The film was very brittle even for this high molecular weight PET, indicating disentanglement between crystallites. Since a low degree of entanglement between folded chain crystals can offer the possibility of a large extension to break while unfolding, we wished to carry out drawing studies on these PET films. This was, however, hindered by the brittleness of the samples, and ductility could be introduced only by annealing between heated plates at 220 °C for 2 min. A lower temperature was not effective in imparting sufficient ductility. Suspecting thermal/hydrolytic degradation of the high molecular weight PET during its solubilization in DPE–BP, and during the subsequent annealing, we carried out IV measurement on the annealed sample. The measured value (2.1 dL/g) was comparable to that of the original sample, indicating no molecular weight degradation. The extent of crystallization of this annealed sample was determined by DSC as 43%, indicating some extent of melting from $x_c =$ 50% (DSC) before the annealing. The thus obtained ductile PET samples could be drawn only at 250 °C to a draw ratio of 5–6 (Section 2.4). A representative stress–strain curve during the subsequent mechanical analysis is shown in Fig. 8. The elastic modulus, breaking strength and elongation to break are $E = 5.3$ GPa, $\sigma_b = 0.35$ GPa and $\varepsilon_b = 9\%$, respectively. In comparison, for a film cast at room

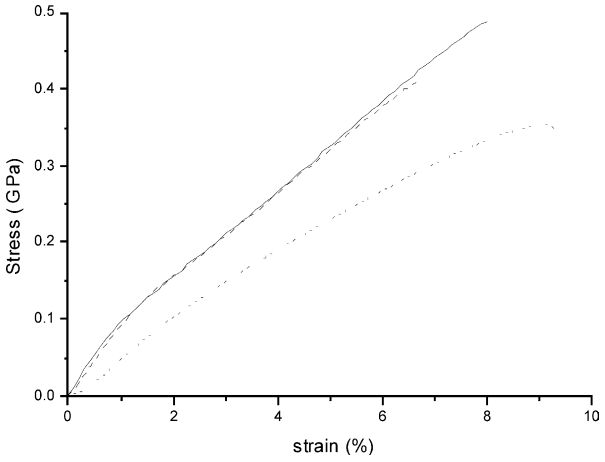

Fig. 8. Tensile behavior of PET crystallized from (a) from HFIP solution through room temperature evaporation (- - -) and drawn 6× at 100 °C and (b) from dilute DPE–BP solution at 170 °C (···), dried, and drawn 5× at 250 °C (c) by pulling filament from concentrated (30 wt%) DPE–BP solution at 250 °C (—), drying, and then drawing 7× at 240 °C.

temperature from the same PET sample's solution (5 wt%) in HFIP, and then drawn to a similar draw ratio, the E, σ_b and ε_b values of were 11, 0.41 GPa and 6.6%. We also carried out filament formation from concentrated PET solution (30 wt%, Section 2.11), followed by overnight drying under vacuum at 150 °C, and then drawing at 240 °C to a draw ratio of 7. The corresponding E, σ_b and ε_b values of were again similar, i.e. 11 GPa, 0.47 GPa and 8% (Fig. 8). Thus, it appears that disentangled crystallization, if any achieved during the crystallization from dilute solution in DPE–BP, was not effective in enhancing the drawability of PET. It could be related to the inherent nature of the strong inter-molecular interaction in PET crystals (e.g. compared to polyethylene) that hinders their unfolding.

4. Conclusions

We have examined the crystallization behavior of very high molecular weight PET from solution in DPE–BP mixture. When in solution (0.25–10%), the PET undergoes crystallization at $T_c \sim 165$ °C during cooling, and melting at $T_m \sim 204$ °C during heating, with the T_c and T_m remaining nearly independent of PET concentration. Though the degree of crystallization is high (~50% by DSC, ~60% by WAXD), the crystallite sizes are somewhat smaller as compared to melt and solid state crystallized PET. Crystallization in dilute solutions (0.25%) results in fibrillar crystals, with the chain alignment perpendicular to the fibril axis. The very high aspect ratio of the crystals is perhaps responsible for the gelation on cooling of even the dilute solutions. Films made from the dilute solution crystallized PET could be drawn five times at 250 °C, resulting in only moderate values of modulus and strength.

References

[1] Schaaf E, Zimmerman H, Dietzel W, Lohmann P. Acta Polym 1981; 32:250.
[2] Ravindranath K, Mashelkar RA. Chem Eng Sci 1986;41:2197.
[3] Chen S-A, Chen F-L. J Polym Sci, Part A: Polym Chem 1987;25:533.
[4] Duh B. J Appl Polym Sci 2002;83:1288.
[5] Marechal E. Polyesters: Synthesis and chemical aspects. In: Fakirov S, editor. Handbook of thermoplastic polyesters, vol. I. New York: Wiley; 2002. p. 1.
[6] Ma Y, Agarwal US, Sikkema DJ, Lemstra PJ. Polymer 2003;44:4085.
[7] Ito M, Takahashi K, Kanamoto T. J Appl Polym Sci 1990;40:1257.
[8] Ziabicki A. Text Res J 1996;66:705.
[9] Huang B, Tucker PA, Cuculo JA. Polymer 1997;38:1101.
[10] Geil PH. Polymer single crystals. New York: Wiley-Interscience; 1963 [chapter IV].
[11] Berghmans H, Cooman RD, Rudder RD, Koningsveld R. Polymer 1998;39:4621.
[12] Keller A. In: Hiltner A, editor. Structure–property relationship of polymeric solids. New York: Plenum Press; 1983.
[13] Lemstra PJ, Krisbaum R. Polymer 1985;26:1372.
[14] Petka WA, Harden JL, McGrath KP, Wirtz D, Tirrell DA. Science 1998;281:389.
[15] Bai S, Hu JZ, Pugmire RJ, Grant DM, Taylor CMV, Rubin JB, et al. Macromolecules 1998;31:9238.
[16] Makarewicz PJ, Wilkes GL. J Polym Sci, Polym Phys Ed 1978;16: 1529.
[17] Jameel H, Noether HD, Rebenfeld L. J Appl Polym Sci 1982;27:773.
[18] Ouyang H, Shore S-H. Polymer 1999;40:5401.
[19] Wang Z-G, Hsiao BS, Fu BX, Liu L, Yeh F, Sauer BB, et al. Polymer 2000;41:1791.
[20] Xue G, Ji G, Li Y. J Polym Sci, Polym Phys 1998;36:1219.
[21] Xue G, Ji G, Yan H, Guo M. Macromolecules 1998;31:7706.
[22] Oh SK, Youg JH, Ha WS. J Korean Fiber Soc 1991;28:52.
[23] Van Veld RD, Morris G, Billica HR. J Appl Polym Sci 1968;12:2709.
[24] Vane LM, Rodriguez F. J Appl Polym Sci 1993;49:765.
[25] Sun B, Lu Y, Ni H, Wang C. Polymer 1998;39:159.
[26] Solomon OF, Ciuta IZ. J Appl Polym Sci 1962;6:683.
[27] Ma Y, Agarwal US, Polymer 2005;46:5447.
[28] Rudder JD, Berghmans H, Roels T, Jacobs A. Colloids Surf A 2001; 183–185:313.
[29] Fakirov S, Fischer EW, Hoffman R, Schmidt GF. Polymer 1977;18: 1121.
[30] Ronald CM. Polym Eng Sci 1991;31:849.
[31] BaltaCalleja FJ, Ohm O, Bayer RK. Polymer 1994;35:4775.
[32] Koncke U, Zachmann HG, BaltaCalleja FJ. Macromolecules 1996;29: 6019.
[33] Fakirov S, Fischer EW, Schmidt GF. Makromol Chem 1975;176: 2459.
[34] Bunn CW. In: Hill R, editor. Fibers from synthetic polymers. Amsterdam: Elsevier; 1953 [chapter 11].
[35] Johnson JE. J Appl Polym Sci 1959;2(5):205.
[36] Von Kilian HG, Halboth H, Jenckel E. Kolloid-Zeitschrift 1960; 172(2):166.
[37] Imai M, Kaji K, Kanaya T. Macromolecules 1994;27:7103.
[38] Atkins EDT, Isaac DH, Keller A, Miyasaka J. J Polym Sci, Polym Phys 1977;15:211.
[39] Hinrichsen G. Die Makromol Chemie 1973;166:291.
[40] Yang X, Tan S, Li G, Zhou E. J Polym Sci, Polym Phys 2001;39:729.
[41] Yang X, Li G, Zhou E. Polymer 2001;42:4713.
[42] Lu XF, Hay JN. Polymer 2001;42:9423.
[43] Aggeli A, Nyrkova IA, Bell M, Harding R, Carrick L, McLeish TCB, et al. Proc Natl Acad Sci 2001;98:11857.
[44] Burkoth TS, Benzinger TLS, Urban V, Lynn DG, Stephen C, Thiyagarajan MP. J Am Chem Soc 1999;121:7429.

[45] Wilson JN, Bangcuyo CG, Erdogan B, Myrick ML, Bunz UHF. Macromolecules 2003;36:1426.
[46] Jun Z, Hou H, Schaper A, Wendorff JH, Greiner A. e-Polymers 2003; 9.
[47] Stephan T, Muth S, Schmidt M. Macromolecules 2002;35:9857.
[48] Jinsan K, Mc Hugh SK, Swager TM. Macromolecules 1999;32:1500.
[49] Pennings AJ. J Polym Sci, Polym Symp 1977;59:55.
[50] Rietveld J, McHugh AJ. J Polym Sci, Polym Phys Ed 1985;23:2339.
[51] Yamaura K, Karaki T, Matsuzawa S. Makromol Chem 1974;175:247.
[52] Pelzbauer Z, Manley RSJ. J Macromol Sci, Phys 1970;4:761.
[53] Xu Y, Zhou E, Yu F, Qian B. Chin J Polym Sci 1988;6:152.
[54] Bolhuis HH, Pennings AJ. J Macromol Sci, Phys 1975;B11:455.
[55] Yamaura K, Yosiroh O, Matsuzawa S. J. Appl Polym Sci, Appl Polym Symp 1985;41:205.
[56] Kimura K, Endo S, Kato Y, Inaba T, Yamashita Y. Macromolecules 1995;28:255.
[57] Shimamura K, Uchida T. J Macromol Sci, Phys 2000;B39:667.
[58] Uemura A, Isoda S, Tsuji M, Ohara M, Kawaguchi A, Katayama K. Bull Inst Chem Res, Kyoto Univ 1986;64(2):66.